International Journal of Chemical, Materials and Biomolecular Sciences
ISSN: 2415-6620
Vol:8, No:11, 2014

Silver Nanoparticles-Enhanced Luminescence Spectra of Silicon Nanocrystals

Khamael M. Abualnaja, Lidija Šiller, Benjamin R. Horrocks

***Abstract*—**Metal-enhanced Luminescence of silicon nanocrystals (SiNCs) was determined using two different particle sizes of silver nanoparticles (AgNPs). SiNCs have been characterized by scanning electron microscopy (SEM), high resolution transmission electron microscopy (HRTEM), Fourier transform infrared spectroscopy (FTIR) and X-ray photoelectron spectroscopy (XPS). It is found that the SiNCs are crystalline with an average diameter of 65 nm and FCC lattice. AgNPs were synthesized using photochemical reduction of $AgNO_3$ with sodium dodecyl sulphate (SDS). The enhanced luminescence of SiNCs by AgNPs was evaluated by confocal Raman microspectroscopy. Enhancement up to ×9 and ×3 times were observed for SiNCs that mixed with AgNPs which have an average particle size of 100 nm and 30 nm, respectively. Silver NPs-enhanced luminescence of SiNCs occurs as a result of the coupling between the excitation laser light and the plasmon bands of AgNPs; thus this intense field at AgNPs surface couples strongly to SiNCs.

***Keywords*—**Luminescence, Silicon Nanocrystals, Silver Nanoparticles, Surface Enhanced Raman Spectroscopy (SERS).

I. Introduction

SEMICONDUCTOR quantum dots are inorganic fluorophores that acquire distinctive photophysical properties which are valuable in an assorted array of applications [1]-[4]. In order to expand the array of applications of inorganic nanoparticles, the combination of dissimilar nanoparticles having dissimilar functions within a complex nanoparticles are used. Multi component composite nanoparticles can show the way towards improvements and enhancements in the luminescence properties of individual inorganic nanoparticles.

SiNCs are being intensively studied because of their potential as luminescent labels [5]. In particular, they may have advantages over the current technology (CdSe quantum dots) in applications where their lack of cytotoxicity and smaller overall size are important factors [6]. Furthermore, a great attention has been focused into Si nanostructures since porous Si exhibit intense visible photoluminescence at room temperature in 1990 [7], [8]. Therefore, the unique optical properties of zero dimensional SiNCs which are different from the bulk silicon open the door to use them in biological sensors and light emitting devices [9]-[14]. It is known that the luminescence characteristics of SiNCs depend upon their size [15] and surface termination [16]. However, Si nanocrystals suffer from the low radiative emission rates because of the indirect band gap of Si which limits the overall brightness of Si nanocrystals [17]-[19]. The indirect nature of the bulk Si band gap and the relatively long (of order 10 μs) radiative lifetimes observed in some preparations have been considered a disadvantage in applications where the PL of each particle is observed for only a short length of time [12], [20]-[25].

There have been several attempts to improve the brightness of SiNCs by the technique of metal enhanced luminescence in which SiNCs are placed in close proximity to metal nanostructures (Ag, Au) which have a strong surface plasmon resonance in the visible spectrum [4], [26], [27]. Metal-enhancement of molecular fluorophores [28]-[31] and quantum dots [3], [32]-[34], including SiNCs [4], [17]-[19], [27] has been reported. The metallic nanoparticles exhibit interesting plasmonics properties which are associated with the interaction between the metal and the incident light which commonly known as localized surface plasmon resonance (LSPR) [35]. This phenomenon only occurs at the boundary between the metal nanostructures and their surrounding environment. The mechanism of this effect is attributed to coupling of the intense local electrical field of the surface plasmon resonance of the metal to the absorption and emission transitions. The surface plasmon resonance of silver and gold nanoparticles give rise to very large absorption coefficients and this alone can increase the brightness of the emitter through an increase in the rate of absorption. This coupling has been found to be stronger when the wavelength of the incident radiation is near to the plasmon resonance of the metal; thus the enhancement of the emission from SiNCs can be observed [36], [37]. Therefore, this phenomenon can be resulted in several optical signal enhancements, such as surface enhanced Raman scattering (SERS), surface enhanced infrared absorption and surface enhanced fluorescence [35], [38]-[41].

When the metal nanoparticles and semiconductor nanostructures are located near to each other and the surface plasmon is resonant with the incident radiation, metal enhanced fluorescence occurs [35], [38]-[41]. It is necessary to choose a metal that provides a strong LSPR at the desired resonance wavelength [42], [43]. AgNPs are considered to be the most interesting metal in plasmonics amongst the noble metal nanoparticles [44]-[46]. This is because AgNPs support narrow LSPR in both visible and near infrared regions i.e. from 300 nm to 1200 nm [44], [47]. Furthermore, AgNPs offer intense SERS enhancements [18], [35]. Taking into accounts

K. M. Abualnaja is with the School of Chemical Engineering and Advanced Materials, Newcastle University, Newcastle Upon Tyne, UK (corresponding author phone: +44 (0) 191 208 5619; e-mail: k.abualnaja@ncl.ac.uk).

L. Šiller is with the School of Chemical Engineering and Advanced Materials, Newcastle University, Newcastle Upon Tyne, UK (e-mail: lidija.siller@ncl.ac.uk).

B. R.Horrocks is with the School of Chemistry, Newcastle University, Newcastle Upon Tyne, UK (e-mail: ben.horrocks@ncl.ac.uk).

the advantages of AgNPs, Ag nanoparticles have been widely used in various applications such as SERS, optics, electronics and photography [35], [48]. However, there is another requirement in order to achieve efficient luminescence enhancement i.e. the incident light should be in resonance with absorption transition of the semiconductor fluorophore. Taking into account this requirement, SiNCs are ideal as their absorption spectrum presents an absorbance which increases gradually above the indirect band gap to reach around 2 eV as observed in SiNCs that prepared by etching Si wafer [49]; subsequently only matching the wavelength of the excitation source with the plasmon mode of the metal is required.

Biteen et al. [18] presented the first evidence of metal enhanced luminesce of SiNCs. They observed that the local-field-enhanced light emission from SiNCs near to film of nanoporous gold. They detected that the intensity of the luminescence from SiNCs enhanced up to four times; as the distance between the nanoporous gold and SiNCs varied from 0 to 20 nm. Biteen et al. [17] then examined metal enhanced luminesce of Si quantum dots using silver island arrays. They determined an enhancement up to seven times in the photoluminescence intensity of SiNCs. Mochiznki et al. [50] observed also the PL intensity of SiNCs enhanced in both types of metal nanoparticles i.e. Ag nanotriangles and Au nanovoids. In particular, the samples that contain Ag nanotriangles have been reported the largest PL enhancement. Recently, Harun and co-authors [4], [51] have observed large enhancement 15-fold for SiNCs encapsulated along with Au nanoparticles in polymer lattices [4]. This enhancement is occurred because the excitation light coupled to the plasmon band of the AuNPs and in turn the intense field at the AuNPs surface couples strongly to the SiNCs. In the absence of AuNPs, they have noticed weak absorption of the SiNCs at the laser wavelength (488) nm and scattering by only the polymer which produces a low PL intensity.

In this work, we report investigation on the metal enhanced luminesce spectra that observed in drop-cast films of SiNCs mixed with silver nanoparticles in two different sizes i.e. 100 nm and 30 nm. First, we describe the experimental methods in Section II, including SiNCs and AgNPs preparations, the structure and chemical characterization of SiNCs using scanning electron microscopy (SEM), high resolution transmission electron microscopy (HRTEM), Fourier transform infrared spectroscopy (FTIR) and X-ray photoelectron spectroscopy (XPS), the optical characterization of SiNCs and their mixtures with AgNPs using UV-visible spectroscopy and confocal Raman microspectroscopy. Then, the results and discussion are presented in Section III. Finally we outline the conclusion in Section IV.

II. Experimental

Commercial SiNCs supplied in the form of a crude powder. Silver nitrate and sodium dodecyl sulphate (SDS) were purchased from Sigma Aldrich. All chemicals were used without further purification. Deionized water was used in all the experiments (nominal resistivity 18 MΩ cm, Nanopure™ purification system, Barnstead).

To obtain well dispersed SiNCs, 3 mg of commercial SiNCs was added to 10 mL of deionized water followed by sonication (Ultrasonic Processor Amplitude) for 10 minutes at 25% of maximum amplitude with a micro tip. Thus, the concentration of commercial SiNCs is 0.3 g/L.

AgNPs were prepared according to the procedure described by Bhaduri et al. [48]. AgNPs were synthesized using silver nitrate salt and SDS which were each dissolved in 100 mL of distilled water separately. The sealed sample vial that contains silver nitrate solution in added SDS solution (200 mL) was exposed to natural sunlight. The sunlight intensities which utilized in this experiment were ≈ 50.3 mW/cm^2 and the sunlight exposure time during the reaction was 1 hour. After around 10 minutes, a change in solution color was noticed from transparent to light brown. Throughout exposure to sunlight, the synthesis temperature of the vial was kept constant at 25°C by using water bath (BS5, Fisher Scientist). The vials of synthesized silver nanoparticles were then kept in the dark. Two kinds of AgNPs samples were prepared which we denote AgNPs (1 mM) and AgNPs (10 mM). For AgNPs (1 mM) the concentration of $AgNO_3$ and SDS were 1 mM and 5 mM, respectively (SDS to $AgNO_3$ molar ratio 5:1). For AgNPs (10 mM) the concentration of $AgNO_3$ and SDS were 10 mM and 50 mM, respectively (SDS to $AgNO_3$ molar ratio fixed at 5:1). The different preparations have substantially different particle sizes of silver NPs because the critical micelle concentration of SDS is about 8 mM under the reaction conditions. The average diameter of AgNPs 1 mM and 10 mM is 100 nm and 30 nm, respectively by HRTEM. Optical absorption spectra of both AgNPs i.e. 1 mM and 10 mM samples showed $\lambda_{max} \simeq 400$ nm.

Scanning electron microscopy (SEM) imaging was done using FEI XL30-ESEM-FEG at Newcastle University in order to measure the size of SiNCs. The sample was prepared by drop-casting 10 μL of SiNCs suspension on aluminum support using a micropipette (Eppendorf) and left overnight to dry in room temperature. SiNCs were then coated with a thin layer of gold to prevent charging before the observation by scanning electron microscopy. High resolution transmission electron microscopy (HRTEM) was carried out at the Materials Science Centre at Manchester University using a Tecnai F30 300 keV microscope. One drop of SiNCs suspension was added on the grids (Agar Scientific) using a micropipette (Eppendorf) and dried overnight in room temperature. To calculate d spacing from HRTEM images, the ImageJ program was used [52]. The Miller indices then were obtained from the chemical database service (CDS) at Daresbury [53].

The chemical characterization of SiNCs was characterized using FTIR and XPS. FTIR measurements were carried out at Newcastle University using a Varian 800 Scimitar Series FTIR over the range of 700-4000 cm^{-1}. The FTIR measurements were performed on SiNCs powder. XPS measurements were carried out at Newcastle University using Kratos Axis Ultra 165 spectrometer with a monochromatic Al K_α X-ray source (photon energy= 1486.6 eV). The pass energy was set at 20.0 eV and 80.0 eV for the survey. A thick film of SiNCs suspension was prepared by a drop cast technique on a

gold substrate using a micropipette (Eppendorf) and left overnight to dry in air at room temperature. The binding energy scale of the spectra was calibrated with reference to the Au $4f_{7/2}$ at 84.0 eV [11]. The background was modelled by a Shirley background and the peaks then were fitted using a mixed singlet function [54].

The optical properties of SiNCs and their mixtures with AgNPs were characterized using UV-Vis spectroscopy (Varian, Cary 100 BIO) at Newcastle University of the wavelength range between 200 to 800 nm using quartz cuvette of 1 cm path length. This measurement was carried out at room temperature. The SiNCs sample was prepared by adding 4 mL of suspension in the quartz cuvette, while the mixtures of SiNCs with metal nanoparticles were prepared by adding 2 mL of AgNPs solution (either 1 mM or 10 mM) to 2 mL of SiNCs in a vial. The mixture was then sonicated for 10 minutes (Hilsonic). 4 mL of the mixture was added to the quartz cuvette.

Silver nanoparticle-enhanced luminescence of SiNCs was measured using confocal microscope (WiTec confocal Raman microscope model CRM200, Ulm, Germany) at Newcastle University. The confocal Raman microscope is used to capture Raman spectra and luminescence images of the following samples: SiNCs and their mixtures with synthesized AgNPs. An Argon ion laser (Melles-Griot) with output power 35 mW at a wavelength of 488 nm was utilized as the excitation source. The collected light was analyzed by a spectrograph equipped with a CCD detector; a grating of 150 lines mm^{-1} was chosen in order to capture the full spectrum including all Raman and luminescence bands of interest. The scan size of all the experiments was 50 x 50 μm in 100 lines at 100 pixels per line with an integration time of 0.1 s/pixel. Samples of SiNCs were prepared by drop-coating 100 μL of the suspension on a glass slide coverslip using a micropipette (Eppendorf). The samples were air dried over night at room temperature and kept in sealed Petri-dishes to avoid contamination. Silver nanoparticles were mixed with SiNCs in order to enable surface enhanced Raman spectroscopy (SERS). These mixtures were prepared by mixing 100 μL of AgNPs (either 1 mM or 10 mM) suspension with 100 μL of SiNCs suspension in centrifuge tube (1.5 mL, Eppendorf). The mixture was then sonicated for 10 minutes (Hilsonic). Then using a micropipette (Eppendorf), 100 μL of the mixture was then drop-coated on a glass slide coverslip. The samples were air dried overnight and kept in sealed Petri-dishes until further analysis.

Three notations were used throughout this work i.e. SiNCs denotes to silicon nanocrystals alone, $+AgNPs_{100}$ and $+AgNPs_{30}$ are mixtures of SiNCs with 1 mM AgNPs and 10 mM AgNPs regarding to their average size, respectively.

III. Results & Discussion

Fig. 1 shows the SEM images of SiNCs dried on an aluminum support. It can be revealed that the particles are spherical in shape and there are agglomerates of SiNCs. Fig. 1 (c) shows the particle size distribution of SiNCs. It can be noticed that there is a large size distribution in SiNCs and the majority of the size of these particles are in range between 20 – 90 nm. The average particle size of SiNCs is ≃ 65 nm.

HRTEM images of SiNCs are shown in Fig. 2. Fig. 2 (a) demonstrates that the SiNCs are crystalline. The calculations of Fast Fourier transform (FFT) on the images of SiNCs were carried out on different regions and showed the presence of the (111) crystal plane (Fig. 2 (a) inset). This diffraction spot that is attributed to the (111) crystal plane corresponds to the face centered cubic (FCC) structure of SiNCs [55]. Agglomerates of SiNCs were detected in HRTEM image as observed also by SEM.

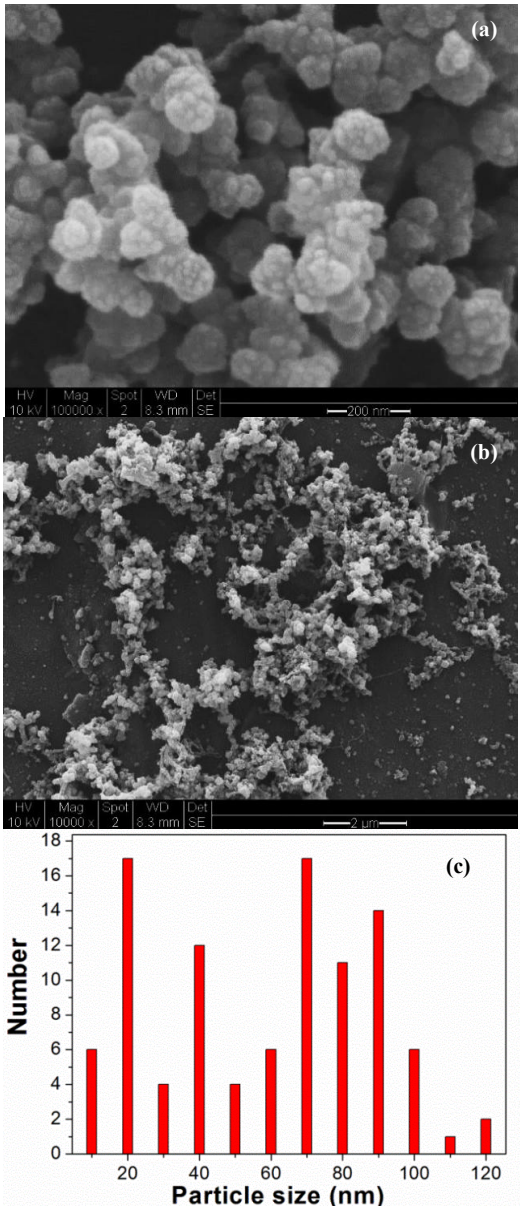

Fig. 1 SEM images of SiNCs dried on an aluminum support present (a) agglomerated SiNCs (b) larger area indicating distribution of SiNCs (c) a histogram of the particle size distribution obtained from 100 Si nanocrystals

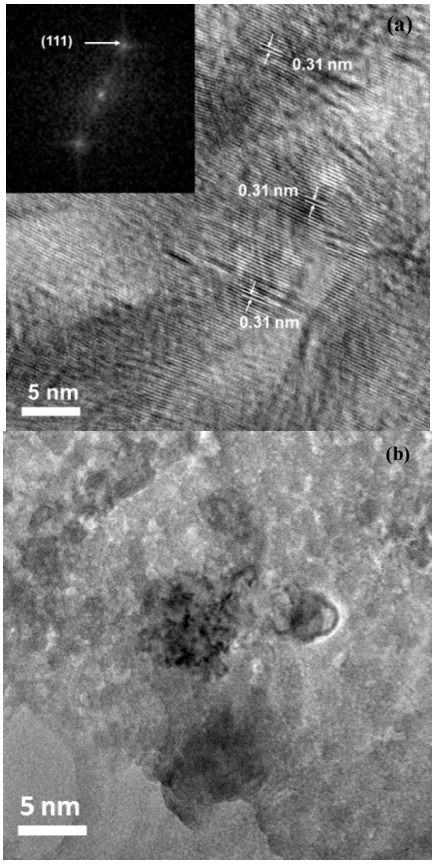

Fig. 2 HRTEM images of SiNCs dried on carbon copper grid showing (a) agglomerated SiNCs (the inset shows the diffraction pattern of SiNCs), (b) agglomeration of SiNCs. The scale bar is 5 nm

Fig. 3 shows the FTIR spectrum of SiNCs. The Si-H_2 bending vibration mode of SiNCs is observed at 620 cm^{-1} [25]. The peak at 860 cm^{-1} attributed to bending vibration mode of Si-O [49]. The IR broad peak at 1080 cm^{-1} correspond to stretching vibration mode of Si-O-Si [25], [56]. The sharp peaks at 1379 cm^{-1} and 1459 cm^{-1} assigned to the bending vibration modes of C-H_2 in SiNCs [49], [56]. The stretching vibration mode of C=O appeared at 1700 cm^{-1} [51]. The sharp IR peaks observed at 2080 cm^{-1} and 2250 cm^{-1} correspond to stretching vibration modes of Si-H and O_3-Si-H, respectively [56]. It can be seen that there are three IR bands of SiNCs in the range 2854-2954 cm^{-1}. The peaks that appear at 2854 cm^{-1} and 2921 cm^{-1} are assigned to the methylene C-H symmetric and asymmetric stretching mode, respectively [49]. While the IR band at 2954 cm^{-1} corresponds to CH_3 stretching mode [49].

Fig. 4 presents the XPS spectra of SiNCs. Fig. 4 (a) shows the XPS spectra of Si2*p* core level for the SiNCs. The broad peak at 103.3 eV with a full width half maximum (FWHM) of 1.5 eV can be assigned to the different species i.e. Si-Si, Si-H and Si-O, thus this peak is a multicomponent peak [11], [21]. As discussed previously, the IR spectrum of SiNCs indicates the presence of Si-H, Si-O. However, the spin orbit splitting of Si*2p* core level here does not appear as a result of the multicomponent nature of this peak. This peak in the Fig. 4 (a) is similar to that reported by Chao et al. [11], [57].

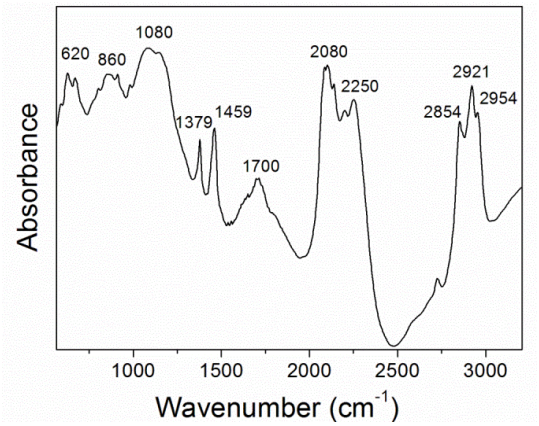

Fig. 3 Fourier transform infrared spectrum of SiNCs

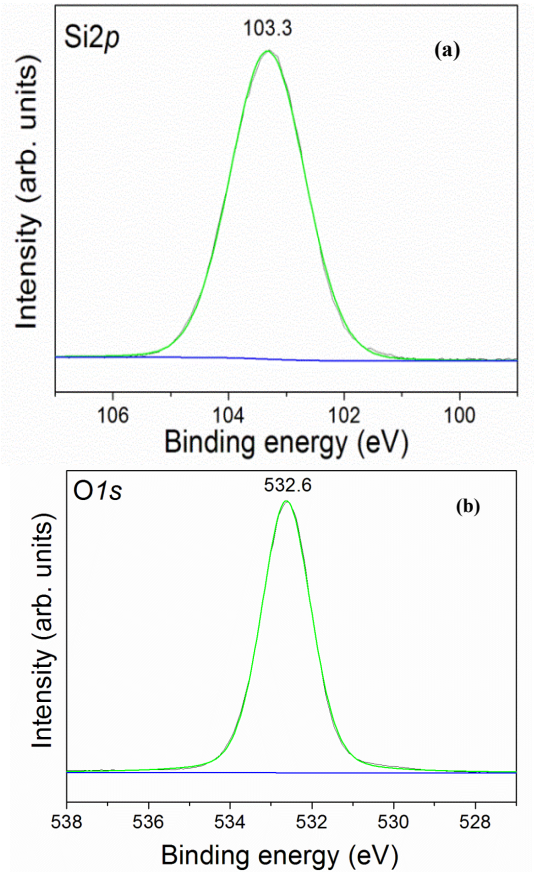

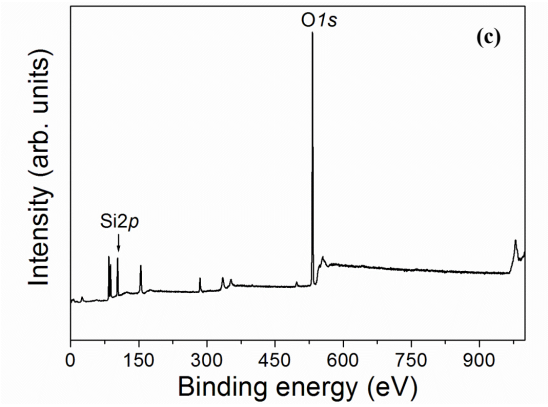

Fig. 4 XPS spectra of SiNCs deposited on gold substrate showing (a) Si*2p*, (b) O*1s* and (c) survey scan

They determined a peak for alkylated silicon nanocrystals at 101.6 eV. Obviously, the difference between these two binding energies is 1.7 eV. This large difference in the binding energy values are predictable because the thickness of the SiNCs film change in every deposition, thus would impact the degree of charging in the film. Corresponding to this peak a similar peak at 532.6 eV with a FWHM of 1.4 eV is observed in the O*1s* spectra (Fig. 4 (b)) that can be attributed to the presence of SiO_x in the film of SiNCs [21]. FTIR study also confirms the presence of SiO_x in the SiNCs sample. Fig. 4 (c) presents a survey spectrum of SiNCs sample. XPS data indicates the presence of Si*2p* and O*1s* core lines which support the FTIR investigation.

Fig. 5 shows the absorption spectra of SiNCs dispersed in deionized water in the wavelength range from 250 nm to 800 nm. It can be seen that the absorption spectra of SiNCs present a broad absorption tail with a steep rise feature at around 350 nm which can be assigned to the direct band gap transition (ca. 3.4 eV in bulk silicon). It is known that bulk silicon exhibits direct band gap of 3.4 eV and an indirect band gap of 1.1 eV [49]. Therefore, there is a rapid increase in the absorbance with decreasing the wavelength from the wavelength of 600 nm (2.06 eV) which presents the absorption band edge of the indirect band gap of SiNCs [49], [58], [59].

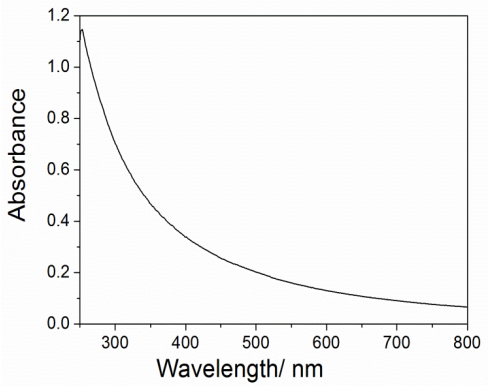

Fig. 5 UV-Vis absorption spectra of SiNCs dispersed in deionized water

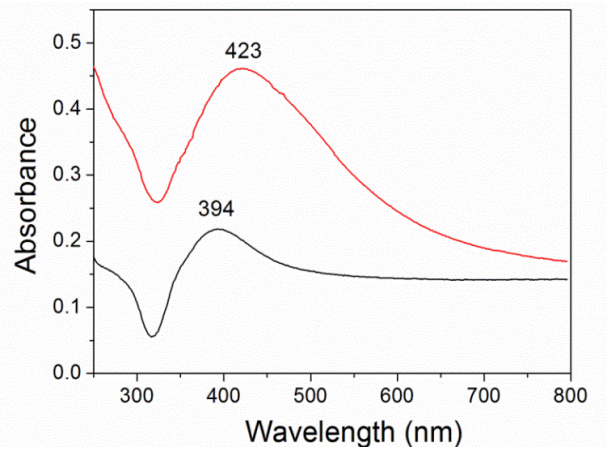

Fig. 6 UV-Vis absorption spectra of SiNCs mixed with $AgNPs_{100}$ (black line) and SiNCs mixed with $AgNPs_{30}$ (red line)

The result shows the absorption increases as the direct gap is approached as observed by Lie et al. [49]. Fig. 6 indicates that the absorption bands of SiNCs mixed with two different particle sizes of AgNPs i.e. 100 nm and 30 nm. The characteristic absorption bands of SiNCs mixed with $AgNPs_{100}$ and $AgNPs_{30}$ appear at 394 nm and 423 nm, respectively. These two peaks are assigned to surface plasmon resonance (SPR) of AgNPs which relies on the particle size of AgNPs and dipole/multipole resonance [48]. The intraband transitions of metallic silver is observed also in AgNPs at ≃ 325 nm [48]. It can be seen that the presences of Si nanoparticles do not affect the plasmon bands of silver nanoparticles.

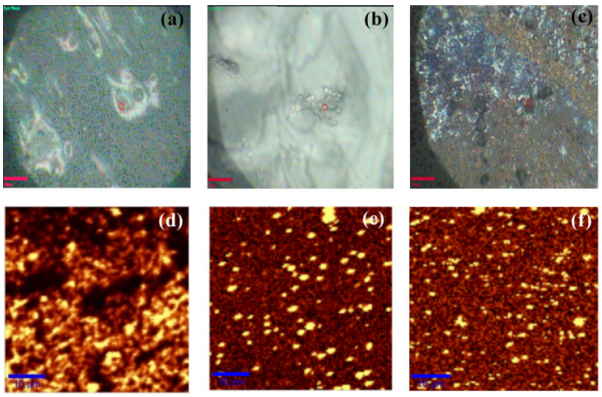

Fig. 7 Reflected light images of (a) SiNCs (b) $+AgNPs_{100}$, (c) $+AgNPs_{30}$ collected before confocal luminescence spectrum images of (d) SiNCs (e) $+AgNPs_{100}$ and (f) $+AgNPs_{30}$ deposited from deionized water on the glass coverslip. The laser wavelength was 488 nm and the scale displays the scattered intensity integrated over the Stokes shift range from 200 cm^{-1} to 7000 cm^{-1}, which corresponds to a mixture of Raman signals and the luminescence. The scale bar of the reflected light images (a-c) is 10 µm and the scan size of the luminescence images (d-f) is 50 X 50 µm

Fig. 7 shows a reflected light images and luminescence images of SiNCs and their mixtures with AgNPs drop-cast on glass coverslip. The confocal luminescence images of dried

SiNCs and their mixtures exhibit bright spots due the presence of clusters of SiNCs. These observed aggregations (clusters) are a result of the drying method that used to prepare the samples. This is because the SEM and HRTEM images of SiNCs present clear evidence that the Si nanoparticles after drying process are aggregated as clusters. Fig. 8 presents the Raman and SERS spectra of SiNCs using 488 nm as an excitation source. Fig. 8 (a) presents the Raman spectrum of SiNCs which drop coated from deionized water onto glass coverslip. The characteristic Raman peak of crystalline Si appears at 520 cm^{-1}. This sharp peak has the same value as bulk crystalline silicon [60], [61]. The Raman feature at 1100 cm^{-1} can be assigned to Si-O vibration mode [62]. The presence of this vibration mode has been also determined in FTIR data of SiNCs. The large and broad peak which detected at 2330 cm^{-1} (550 nm) refers to the luminescence signals of SiNCs. It is surprisingly that the commercial SiNCs luminescence regarding to the size of SiNCs which have an average diameter of 65 nm. This can be due to (i) the presence of small fraction of small particles size (their radius ⍰ Bohr radius) of commercial SiNCs which SEM and HRTEM techniques cannot detect them and (ii) the presence of small grains which are responsible for the luminescence of Si nanoparticles. The second reason should be ruled out as there are no grains observed in HRTEM image of commercial SiNCs. Thus, the first reason is most likely to be the main responsible of the luminescence in commercial SiNCs in this study. Figs. 8 (b), (c) show the SERS features of SiNCs with metal NPs, the signals in the region 350–630 cm^{-1} can be attributed to SO_3 stretching vibrational modes of SDS which used as a reducing agent to synthesis AgNPs [63]. The $–CH_2$-bending vibrations modes of the carbon chain of the SDS molecule are in the region 1350–1580 cm^{-1} [63]. The SERS peaks at around 2900 cm^{-1} can be assigned to C-H stretching vibrations modes of the carbon group of dodecyl sulphate molecule [63].

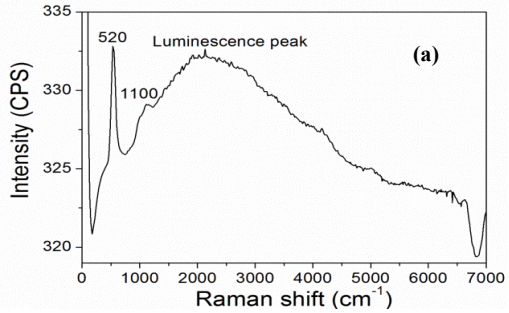

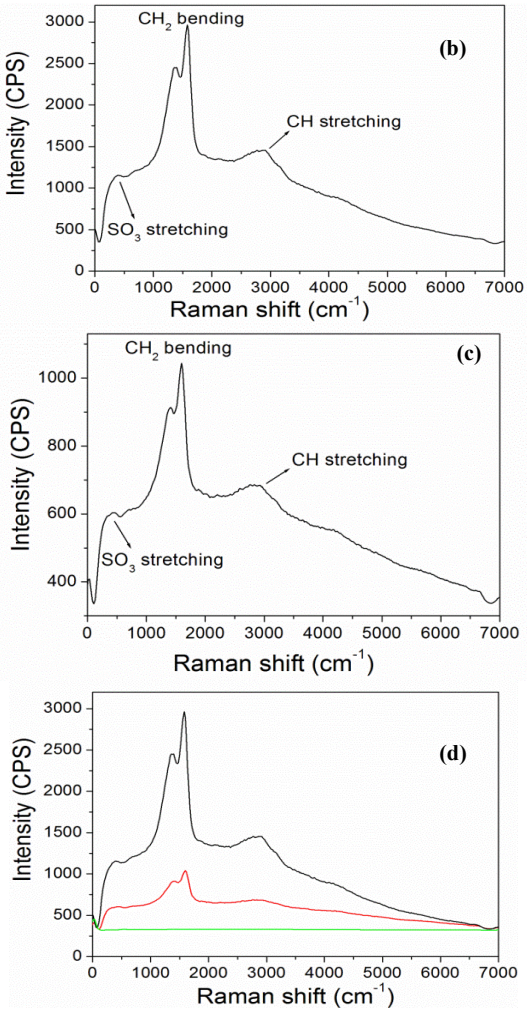

Fig. 8 Average Raman and luminescence spectra of (a) SiNCs, (b) +$AgNPs_{100}$, (c) +$AgNPs_{30}$ and (d) comparing (a), (b) and (c) together. All samples were drop-coated from aqueous solution on glass coverslips. The excitation wavelength = 488 nm line of an argon ion laser was used to excite the luminescence and the spectra was collected using a grating = 150 lines mm^{-1} which provides collection of both Raman and luminescence from silicon nanocrystals. The elastically scattered laser light is observed as a higher intensity peak at 0 cm^{-1}

It is clear that the typical luminescence peak of SiNCs does not disappear but it is dominated by much larger peak at lower wavelength at around 500–4000 cm^{-1}. Thus, this luminescence peak blue shifted in presence of $AgNPs_{100}$ and $AgNPs_{30}$. This blue shift can be explained as a result of the presence of metal nanoparticles i.e. AgNPs. In the presence of metal nanoparticles, the 488 nm light which used as an excitation source mostly does not excite the SiNCs directly, but is absorbed by the plasmon band and the near field of the plasmon couples to the SiNCs and excites it. However, the near field is only strong (near) to the metal, i.e. on the surface of the SiNCs. It is then logical the emission would be blue-shifted because only close to surface states not core states are excited. On the other hand, our group was observed that

oxide-rich parts of alkylated silicon quantum dots may have localized states that emit light blue shifted compared to un-oxidized parts of the particle on the surface [64]. Therefore, the effect of trace oxides on the surface of SiNCs is important and known to cause a blue shift in this study. Also, Zidek et al. [65], [66] discuss the effect of the surface on the emitting state as there may be many, slightly different emitting states even in a single particle. The second possible explanation for this blue shift is the coupling of the localized surface plasmon resonance (LSPR) to states near the direct gap of SiNCs, which radiative more efficiently. The reason that LSPR couples efficiently to such states may be simply that the wavelength of the laser i.e. 488 nm and LSPR near 400 nm are very blue compared to the orange luminescence at the indirect gap.

It is clear that the simple mixtures of SiNCs with silver nanoparticles yield substantial increases in the intensity of emitted/scattered light as seen in Fig. 8. The presence of $AgNPs_{100}$ and $AgNPs_{30}$ in a mixture with SiNCs produces enhancement on the PL intensity of the most intense band (CH_2 bending vibration mode) up to ×9 and ×3 times, respectively as compared to the conventional SiNCs (see Fig. 8 (d)). The normal explanation for the PL enhancement by AgNPs is in terms of the efficient coupling between the excitation laser light (488 nm) and the plasmon bands of AgNPs; thus this intense field at AgNPs surface couples strongly to SiNCs. Silicon NCs have a relatively low absorbance at 488 nm, but the absorption coefficient of Ag nanoparticles near the plasmon resonance is known to be very large and so long as the SiNCs are within the range of the near-field at the metal surface, the rate of absorption can be much greater. However, there is obvious difference in PL intensities enhancement of SiNCs with AgNPs as shown in Fig. 8 (d). Taking into account the particle sizes of AgNPs, it is clear that the PL enhancement of $+gNPs_{100}$ sample is higher than $+AgNPs_{30}$ sample which reflect the strong interaction between the localized surface plasmon resonance of $AgNPs_{100}$ and the electric field forming a strong polarization near SiNCs. Our phenomena is in agreement with the study that reported by Rycenga et al. [35] They have found that varying the dimension of AgNPs will influence the scattering and the absorption peak of localized surface plasmon resonance (LSPR). They have suggested that when AgNPs have diameter about 30 nm the absorption is more dominant compared to scattering. Whereas, the AgNPs with size range from 40 nm to 140 nm had a significantly higher scattering intensity compared to the absorption. The second possible interpretation of this difference enhancement in the PL intensities may be related to the concentration of AgNPs. When the concentration of AgNPs increased from 1 Mm to 10 Mm, AgNPs tend to self-aggregate. Subsequently, these clusters will reduce the luminescence intensity of AgNPs. This explanation is compatible with SEM images of synthesized AgNPs 1 Mm and 10 Mm which observed further agglomeration for Ag nanoparticles in higher concentration [48]. This observation also is consistent with that observed by Chandra et al. [67]. They have found that increasing the metallic nanoparticles concentrations will reduce the emission intensity of CdSe/ZnS QDs.

IV. Conclusion

SEM and HRTEM results indicate that the SiNCs are crystalline with an average diameter of 65 nm and FCC lattice. SiNCs show enhanced luminescence when mixed with AgNPs. The enhanced luminescence of SiNCs by AgNPs was evaluated by confocal Raman microspectroscopy. Enhancement up to ×9 and ×3 times were observed for SiNCs that mixed with AgNPs which have an average particle size of 100 nm and 30 nm, respectively. Silver NPs-enhanced luminescence of SiNCs occurs as a result of the coupling between the excitation laser light and the plasmon bands of AgNPs; thus this intense field at AgNPs surface couples strongly to SiNCs.

Acknowledgment

We would like to thank Taif University and the Ministry of Higher Education, Saudi Arabia.

References

[1] T.-H. Chen, K.-W. Kuo, W.-T. Kuo, H.-Y. Huang, Y.-Y. Huang, Quantum Dots Combined with Nanogold to Detect the Delivery Routes of Particles into Cells, Journal of Bionanoscience, 2 (2008) 109-113.

[2] R. Bakalova, Z. Zhelev, H. Ohba, Y. Baba, Quantum Dot-Conjugated Hybridization Probes for Preliminary Screening of siRNA Sequences, Journal of the American Chemical Society, 127 (2005) 11328-11335.

[3] Y. Fu, J. Zhang, J.R. Lakowicz, Silver-enhanced fluorescence emission of single quantum dot nanocomposites, Chemical Communications, (2009) 313-315.

[4] N.A. Harun, M.J. Benning, B.R. Horrocks, D.A. Fulton, Gold nanoparticle-enhanced luminescence of silicon quantum dots co-encapsulated in polymer nanoparticles, Nanoscale, 5 (2013) 3817-3827.

[5] F. Erogbogbo, K.T. Yong, I. Roy, G.X. Xu, P.N. Prasad, M.T. Swihart, Biocompatible luminescent silicon quantum dots for imaging of cancer cells, ACS Nano, 2 (2008) 873-878.

[6] N.H. Alsharif, C.E.M. Berger, S.S. Varanasi, Y. Chao, B.R. Horrocks, H.K. Datta, Alkyl-Capped Silicon Nanocrystals Lack Cytotoxicity and have Enhanced Intracellular Accumulation in Malignant Cells via Cholesterol-Dependent Endocytosis, Small, 5 (2009) 221-228.

[7] L.T. Canham, Silicon quantum wire array fabrication by electrochemical and chemical dissolution of wafers, Applied Physics Letters, 57 (1990) 1046-1048.

[8] A. Cullis, L.T. Canham, P. Calcott, The structural and luminescence properties of porous silicon, J. Appl. Phys., 82 (1997) 909-965.

[9] N. O'Farrell, A. Houlton, B.R. Horrocks, Silicon nanoparticles: applications in cell biology and medicine, Int. J. Nanomed., 1 (2006) 451-472.

[10] Y. Chao, A. Houlton, B.R. Horrocks, M.R.C. Hunt, N.R.J. Poolton, J. Yang, L. Siller, Optical luminescence from alkyl-passivated Si nanocrystals under vacuum ultraviolet excitation: Origin and temperature dependence of the blue and orange emissions, Applied Physics Letters, 88 (2006) 263119-263119-263113.

[11] Y. Chao, S. Krishnamurthy, M. Montalti, L.H. Lie, A. Houlton, B.R. Horrocks, L. Kjeldgaard, V.R. Dhanak, M.R.C. Hunt, L. Šiller, Reactions and luminescence in passivated Si nanocrystallites induced by vacuum ultraviolet and soft-x-ray photons, Journal of Applied Physics, 98 (2005) -.

[12] R.J. Rostron, Y. Chao, G. Roberts, B.R. Horrocks, Simultaneous photocharging and luminescence intermittency in silicon nanocrystals, Journal of Physics Condensed Matter, 21 (2009).

[13] A.M. Smith, S. Nie, Semiconductor Nanocrystals: Structure, Properties, and Band Gap Engineering, Accounts of Chemical Research, 43 (2009) 190-200.

[14] A.M. Hartel, S. Gutsch, D. Hiller, C. Kübel, N. Zakharov, P. Werner, M. Zacharias, Silicon nanocrystals prepared by plasma enhanced chemical

vapor deposition: Importance of parasitic oxidation for third generation photovoltaic applications, Applied Physics Letters, 101 (2012) -.
[15] T. Fischer, V. Petrova-Koch, K. Shcheglov, M.S. Brandt, F. Koch, Continuously tunable photoluminescence from Si+-implanted and thermally annealed SiO2 films, Thin Solid Films, 276 (1996) 100-103.
[16] M.V. Wolkin, J. Jorne, P.M. Fauchet, G. Allan, C. Delerue, Electronic States and Luminescence in Porous Silicon Quantum Dots: The Role of Oxygen, Physical Review Letters, 82 (1999) 197-200.
[17] J.S. Biteen, N.S. Lewis, H.A. Atwater, H. Mertens, A. Polman, Spectral tuning of plasmon-enhanced silicon quantum dot luminescence, Applied Physics Letters, 88 (2006) 131109-131109-131103.
[18] J.S. Biteen, D. Pacifici, N.S. Lewis, H.A. Atwater, Enhanced Radiative Emission Rate and Quantum Efficiency in Coupled Silicon Nanocrystal-Nanostructured Gold Emitters, Nano Letters, 5 (2005) 1768-1773.
[19] J.S. Biteen, L.A. Sweatlock, H. Mertens, N.S. Lewis, A. Polman, H.A. Atwater, Plasmon-Enhanced Photoluminescence of Silicon Quantum Dots: Simulation and Experiment, The Journal of Physical Chemistry C, 111 (2007) 13372-13377.
[20] H. Li, D. Xu, G. Guo, L. Gui, Y. Tang, X. Ai, Z. Sun, X. Zhang, G.G. Qin, Intense and stable blue-violet emission from porous silicon modified with alkyls, Journal of Applied Physics, 88 (2000) 4446-4448.
[21] J.C. Vial, A. Bsiesy, F. Gaspard, R. Hérino, M. Ligeon, F. Muller, R. Romestain, R.M. Macfarlane, Mechanisms of visible-light emission from electro-oxidized porous silicon, Physical Review B, 45 (1992) 14171-14176.
[22] Y.H. Xie, W.L. Wilson, F.M. Ross, J.A. Mucha, E.A. Fitzgerald, J.M. Macaulay, T.D. Harris, Luminescence and structural study of porous silicon films, Journal of Applied Physics, 71 (1992) 2403-2407.
[23] D.I. Kovalev, I.D. Yaroshetzkii, T. Muschik, V. Petrova-Koch, F. Koch, Fast and slow visible luminescence bands of oxidized porous Si, Applied Physics Letters, 64 (1994) 214-216.
[24] J. Linnros, N. Lalic, A. Galeckas, V. Grivickas, Analysis of the stretched exponential photoluminescence decay from nanometer-sized silicon crystals in SiO2, Journal of Applied Physics, 86 (1999) 6128-6134.
[25] G.M. Credo, M.D. Mason, S.K. Buratto, External quantum efficiency of single porous silicon nanoparticles, Applied Physics Letters, 74 (1999) 1978-1980.
[26] D.M. Schaadt, B. Feng, E.T. Yu, Enhanced semiconductor optical absorption via surface plasmon excitation in metal nanoparticles, Applied Physics Letters, 86 (2005) -.
[27] H. Mertens, J.S. Biteen, H.A. Atwater, A. Polman, Polarization-Selective Plasmon-Enhanced Silicon Quantum-Dot Luminescence, Nano Letters, 6 (2006) 2622-2625.
[28] W. Trabesinger, A. Kramer, M. Kreiter, B. Hecht, U.P. Wild, Single-molecule near-field optical energy transfer microscopy, Applied Physics Letters, 81 (2002) 2118-2120.
[29] A. Kramer, W. Trabesinger, B. Hecht, U. Wild, Optical near-field enhancement at a metal tip probed by a single fluorophore, Applied Physics Letters, 80 (2002) 1652-1654.
[30] E. Dulkeith, M. Ringler, T.A. Klar, J. Feldmann, A. Muñoz Javier, W.J. Parak, Gold Nanoparticles Quench Fluorescence by Phase Induced Radiative Rate Suppression, Nano Letters, 5 (2005) 585-589.
[31] P. Anger, P. Bharadwaj, L. Novotny, Enhancement and Quenching of Single-Molecule Fluorescence, Physical Review Letters, 96 (2006) 113002.
[32] K. Ray, R. Badugu, J.R. Lakowicz, Metal-Enhanced Fluorescence from CdTe Nanocrystals: A Single-Molecule Fluorescence Study, Journal of the American Chemical Society, 128 (2006) 8998-8999.
[33] K. Okamoto, S. Vyawahare, A. Scherer, Surface-plasmon enhanced bright emission from CdSe quantum-dot nanocrystals, Journal of the Optical Society of America B, 23 (2006) 1674-1678.
[34] O. Kulakovich, N. Strekal, A. Yaroshevich, S. Maskevich, S. Gaponenko, I. Nabiev, U. Woggon, M. Artemyev, Enhanced Luminescence of CdSe Quantum Dots on Gold Colloids, Nano Letters, 2 (2002) 1449-1452.
[35] M. Rycenga, C.M. Cobley, J. Zeng, W. Li, C.H. Moran, Q. Zhang, D. Qin, Y. Xia, Controlling the Synthesis and Assembly of Silver Nanostructures for Plasmonic Applications, Chemical Reviews, 111 (2011) 3669-3712.
[36] J. Gersten, A. Nitzan, Spectroscopic properties of molecules interacting with small dielectric particles, The Journal of Chemical Physics, 75 (1981) 1139-1152.
[37] A.D. McFarland, M.A. Young, J.A. Dieringer, R.P. Van Duyne, Wavelength-Scanned Surface-Enhanced Raman Excitation Spectroscopy, The Journal of Physical Chemistry B, 109 (2005) 11279-11285.
[38] B. Wiley, Y. Sun, B. Mayers, Y. Xia, Shape-Controlled Synthesis of Metal Nanostructures: The Case of Silver, Chemistry – A European Journal, 11 (2005) 454-463.
[39] A.M. Schwartzberg, J.Z. Zhang, Novel Optical Properties and Emerging Applications of Metal Nanostructures†, The Journal of Physical Chemistry C, 112 (2008) 10323-10337.
[40] W.L. Barnes, A. Dereux, T.W. Ebbesen, Surface plasmon subwavelength optics, Nature, 424 (2003) 824-830.
[41] W.A. Murray, W.L. Barnes, Plasmonic Materials, Advanced Materials, 19 (2007) 3771-3782.
[42] S. Link, M.B. Mohamed, M.A. El-Sayed, Simulation of the Optical Absorption Spectra of Gold Nanorods as a Function of Their Aspect Ratio and the Effect of the Medium Dielectric Constant, The Journal of Physical Chemistry B, 103 (1999) 3073-3077.
[43] S. Lal, S. Link, N.J. Halas, Nano-optics from sensing to waveguiding, Nat Photon, 1 (2007) 641-648.
[44] B. Wiley, Y. Sun, Y. Xia, Synthesis of Silver Nanostructures with Controlled Shapes and Properties, Accounts of Chemical Research, 40 (2007) 1067-1076.
[45] A.L. Pyayt, B. Wiley, Y. Xia, A. Chen, L. Dalton, Integration of photonic and silver nanowire plasmonic waveguides, Nat Nano, 3 (2008) 660-665.
[46] M. Rang, A.C. Jones, F. Zhou, Z.-Y. Li, B.J. Wiley, Y. Xia, M.B. Raschke, Optical Near-Field Mapping of Plasmonic Nanoprisms, Nano Letters, 8 (2008) 3357-3363.
[47] E.L. Ru, P. Etchegoin, Principles of Surface-Enhanced Raman Spectroscopy: and related plasmonic effects, Elsevier Science, 2008.
[48] G.A. Bhaduri, R. Little, R.B. Khomane, S.U. Lokhande, B.D. Kulkarni, B.G. Mendis, L. Šiller, Green synthesis of silver nanoparticles using sunlight, Journal of Photochemistry and Photobiology A: Chemistry, 258 (2013) 1-9.
[49] L.H. Lie, M. Duerdin, E.M. Tuite, A. Houlton, B.R. Horrocks, Preparation and characterisation of luminescent alkylated-silicon quantum dots, Journal of Electroanalytical Chemistry, 538–539 (2002) 183-190.
[50] Y. Mochizuki, M. Fujii, S. Hayashi, T. Tsuruoka, K. Akamatsu, Enhancement of photoluminescence from silicon nanocrystals by metal nanostructures made by nanosphere lithography, J. Appl. Phys., 106 (2009).
[51] N.A. Harun, B.R. Horrocks, D.A. Fulton, Enhanced Raman and luminescence spectra from co-encapsulated silicon quantum dots and Au-Ag nanoalloys, Chemical Communications, (2014).
[52] M. Picquart, Vibrational model behavior of SDS aqueous solutions studied by Raman scattering, The Journal of Physical Chemistry, 90 (1986) 243-250.
[53] CDS. Chemical Database Service, Daresbury, in, 2014.
[54] D.A. Shirley, High-Resolution X-Ray Photoemission Spectrum of the Valence Bands of Gold, Physical Review B, 5 (1972) 4709-4714.
[55] S.M. Barnett, N. Harris, J.J. Baumberg, Molecules in the mirror: how SERS backgrounds arise from the quantum method of images, Physical Chemistry Chemical Physics, 16 (2014) 6544-6549.
[56] L.J. Bellamy, The Infra-red Spectra of Complex Molecules, Chapman and Hall, 1975.
[57] Y. Chao, L. Siller, S. Krishnamurthy, P.R. Coxon, U. Bangert, M. Gass, L. Kjeldgaard, S.N. Patole, L.H. Lie, N. O'Farrell, T.A. Alsop, A. Houlton, B.R. Horrocks, Evaporation and deposition of alkyl-capped silicon nanocrystals in ultrahigh vacuum, Nat Nano, 2 (2007) 486-489.
[58] K.A. Littau, P.J. Szajowski, A.J. Muller, A.R. Kortan, L.E. Brus, A luminescent silicon nanocrystal colloid via a high-temperature aerosol reaction, The Journal of Physical Chemistry, 97 (1993) 1224-1230.
[59] T. Mohanty, N.C. Mishra, A. Pradhan, D. Kanjilal, Luminescence from Si nanocrystal grown in fused silica using keV and MeV beam, Surface and Coatings Technology, 196 (2005) 34-38.
[60] G. Faraci, S. Gibilisco, P. Russo, A.R. Pennisi, S. La Rosa, Modified Raman confinement model for Si nanocrystals, Physical Review B, 73 (2006).
[61] Y. Duan, J.F. Kong, W.Z. Shen, Raman investigation of silicon nanocrystals: quantum confinement and laser-induced thermal effects, Journal of Raman Spectroscopy, 43 (2012) 756-760.
[62] L.V. Mercaldo, E.M. Esposito, P.D. Veneri, G. Fameli, S. Mirabella, G. Nicotra, First and second-order Raman scattering in Si nanostructures within silicon nitride, Applied Physics Letters, 97 (2010).

[63] G. Cazzolli, S. Caponi, A. Defant, C.M.C. Gambi, S. Marchetti, M. Mattarelli, M. Montagna, B. Rossi, F. Rossi, G. Viliani, Aggregation processes in micellar solutions: a Raman study, Journal of Raman Spectroscopy, 43 (2012) 1877-1883.
[64] F.M. Dickinson, T.A. Alsop, N. Al-Sharif, C.E.M. Berger, H.K. Datta, L. Siller, Y. Chao, E.M. Tuite, A. Houlton, B.R. Horrocks, Dispersions of alkyl-capped silicon nanocrystals in aqueous media: photoluminescence and ageing, Analyst, 133 (2008) 1573-1580.
[65] K. Žídek, I. Pelant, F. Trojánek, P. Malý, P. Gilliot, B. Hönerlage, J. Oberlé, L. Šiller, R. Little, B.R. Horrocks, Ultrafast stimulated emission due to quasidirect transitions in silicon nanocrystals, Physical Review B, 84 (2011) 085321.
[66] K. ídek, F. Trojánek, P. Malý, L. Ondi, I. Pelant, K. Dohnalová, L. iller, R. Little, B.R. Horrocks, Femtosecond luminescence spectroscopy of core states in silicon nanocrystals, Optics Express, 18 (2010) 25241-25249.
[67] S. Chandra, J. Doran, S.J. McCormack, M. Kennedy, A.J. Chatten, Enhanced quantum dot emission for luminescent solar concentrators using plasmonic interaction, Sol. Energy Mater. Sol. Cells, 98 (2012) 385-390.